JOURNAL OF SOLID STATE CHEMISTRY 30, 89–105 (1979)

Magnetic and Spectroscopic Investigation of Partially Reduced Vanadium Pentoxides. I. α-$Cu_xV_2O_5$*

F. Y. ROBB AND W. S. GLAUNSINGER†

Department of Chemistry, Arizona State University, Tempe, Arizona 85281

Received June 28, 1978; in revised form November 3, 1978

The electron paramagnetic resonance (EPR) and magnetic susceptibility of both powdered and crystalline α-$Cu_xV_2O_5$ near the compositional limit have been studied as a function of temperature. The EPR data indicate that the paramagnetic species are isolated V^{4+} centers in a nearly axially symmetric ligand field. It is demonstrated that reasonably precise EPR parameters can be derived from powdered spectra. The narrowness of the EPR line suggests that the spectra are motionally narrowed via thermally activated hopping of the paramagnetic electron of V^{4+}. Expressions are derived for the temperature-dependent magnetic moments of the octahedral $^2T_{2g}$ term under the combined perturbation of spin–orbit coupling and an axially symmetric ligand field, and the susceptibility data are interpreted in terms of this model. It is found that the sixfold degenerate $^2T_{2g}$ level is split into three levels with the lowest and highest levels possessing a magnetic moment and the intermediate level having no moment. This model is also consistent with the g-tensor and can account for the temperature dependence of the EPR linewidth.

Introduction

The key to oxidation catalysis by V_2O_5 is its ability to undergo partial reduction. Partially reduced, nonstoichiometric V_2O_5 can be produced in a variety of ways, such as incorporation of altervalent metals, oxygen deficiency, and addition of glass-formers. In particular, monovalent cations such as Li^+ and Na^+ occupy interstitial sites (*1*). The host orthorhombic V_2O_5 structure is maintained for low values of x (α phase) (*2*); however, at higher x values a series of monoclinic vanadium bronzes (β phase) is produced (*3*).

The slightly reduced, α phase of V_2O_5 has several interesting properties. The electrical (*4*) and electron paramagnetic resonance (EPR) (*5*) behavior in these materials shows that the interstitial monovalent metal donates its valence electron to the vanadium sites, which reduces the valence of vanadium form V to IV, i.e., $M + V^{5+} \rightarrow M^+ + V^{4+}$. Furthermore, the d electron on V^{4+} is not always localized, but moves among the vanadium sites by a thermally activated hopping process (*6*). It is likely that the localization mechanism involves small-polaron formation, possibly aided by the interaction of the d electron with the non-periodic Coulomb field of the monovalent cations (*7*).

The α phase had been extensively investigated by EPR (*5–9*). The results of these studies are frequently not in agreement, probably because the compositions were not determined accurately and because of the variety of localized vanadium centers that can be formed. Although previous studies do agree that the unpaired electron is localized on vanadium sites and that the resulting paramagnetic center has axial symmetry,

* This research was supported in part by Grant DMR 75-09215 from the National Science Foundation.

† To whom to address inquiries.

0022-4596/79/100089-17 $02.00/0

they disagree over the number of different vanadium centers and the extent of electronic delocalization for these centers.

Although the crystal structures of the α and β phases are different, both structures have similar distorted VO_6 octahedra and similar V–O and closest V–V distances. Hence the properties of the α phase should resemble those of the more extensively investigated β phase. For example, in both phases the paramagnetism is due to V^{4+} and electronic transport occurs via thermally activated hopping (*10*). In addition, the electronic energy levels may be similar, in which case the V^{4+} ground state in the α phase may be nonmagnetic (*11*). However, this latter conclusion is only tentative since the β phase magnetic analysis has been criticized by Goodenough *(12)*.

The present study of well-characterized powdered and crystalline α-$Cu_xV_2O_5$ was undertaken in an attempt to obtain a comprehensive set of magnetic and EPR data whose interpretation would lead to a self-consistent model of the paramagnetic behavior of these materials. The compositions were chosen near the limit of α-phase stability to enhance the sensitivity of the magnetic measurements and to possibly produce results which may be applicable to the β-phase vanadium bronzes. It is hoped that a detailed knowledge of the magnetic properties of slightly reduced V_2O_5 may be of use in understanding the role of V_2O_5 in oxidation catalysis.

Experimental

Sample Preparation and Characterization

The α phase of $Cu_xV_2O_5$ was prepared by reacting Cu with V_2O_5 according to the equation:

$$xCu + V_2O_5 \rightarrow Cu_xV_2O_5. \qquad (1)$$

Specpure Johnson–Matthey Cu and V_2O_5 were used in all preparations. Powder samples were prepared by heating a mixture of powdered Cu and V_2O_5 to 600°C for 24 hr. The product was reground and refired five times to ensure sample homogeneity. Single crystals were prepared by melting a mixture of Cu and V_2O_5 in a platinum crucible followed by programmed cooling of the melt. Typically, the melt was held at about 780°C for 24 hr and then cooled at a rate of 2–5°C/hr.

Powder X-ray diffraction of all samples with $x \lesssim 0.02$ was identical with that of V_2O_5. Electron microprobe analysis was used to determine sample homogeneity and chemical composition. V_2O_5 and Cu_2O single crystals were used as standards. A Cameca MS-46 microprobe equipped with four single-crystal-wavelength X-ray spectrometers and one energy-dispersive spectrometer (EDS) was used. The EDS scan (0.2% detection limit) showed no secondary phases present. Although the compositions of the powder preparations were always close to the starting composition, the crystalline composition generally deviated significantly from the original composition, which is probably due to an inhomogeneous melt. The powder and crystalline samples chosen for detailed study had x values of 0.0100 and 0.0140, respectively.

EPR Measurements

Variable-temperature EPR spectra were recorded using an X-band reflection spectrometer and variable-temperature equipment described elsewhere (*13, 14*). Both the first and second derivative of the EPR absorption were recorded. After cleaning and mounting the crystal, it could be aligned in the EPR spectrometer within 2° of the crystallographic axes. A calibrated, adjustable single-crystal ruby standard positioned near the sample in the microwave cavity was used as an intensity standard and to calibrate large field sweeps (*15*). Accurate g-factors were measured using charred dextrose as an internal standard (*16*). Although a weak

resonance is observed in pure V_2O_5, this resonance is about 25 times less intense than that in the samples and hence makes a negligible contribution to the observed spectra.

Magnetic Susceptibility Measurements

The magnetic susceptibility was measured in a Faraday apparatus. The maximum field was 13 kG, with $H(dH/dz) = 27$ (kG)^2/cm. The setup was calibrated with platinum and $HgCo(SCN)_4$. Crystals could be aligned in the susceptibility apparatus within about 4° of the crystallographic axes. At each temperature the susceptibility was determined at eight field strengths ranging from 2.5 to 13 kG. All susceptibilities have been extrapolated to zero reciprocal field and then corrected for ionic diamagnetism and host susceptibility to obtain the reported values.

Results

A. EPR

1. Crystalline $Cu_{0.014}V_2O_5$. Typical EPR spectra for the field parallel and perpendicular to the crystallographic *b* axis at 296°K are shown in Fig. 1. The lineshape is Lorentzian at all crystal orientations. The angular variation of the EPR spectra can be described by the spin Hamiltonian:

$$\beta(g_xH_x\hat{S}_x + g_yH_y\hat{S}_y + g_zH_z\hat{S}_z), \qquad (2)$$

where within experimental error (±2°) the crystallographic *a*, *c*, and *b* axes coincide with the principal *x*, *y*, and *z* axes, respectively, of the *g*-tensor. The angular variations of the EPR spectra are shown in Figs. 2 and 3, and the principal *g*-values at 296°K are summarized in Table I. The *g*-values are in good agreement with a previous EPR study of $Cu_{0.01}V_2O_5$ (*7*). It is evident that the *g*-tensor is axially symmetric, with *b* being the unique magnetic axis. The *g*-tensor was indpendent of temperature to ±0.01 between liquid-helium and ambient temperatures. At this composition we have found no evidence for different vanadium centers (*5*) or electronic delocalization over more than one vanadium ion (*5–7*), found by others at lower *x* values.

Interestingly, the linewidth is dependent on orientation, varying from about 60 G for $H \| b$ to 40 G for $H \perp b$, as shown in Fig. 4. The temperature dependence of the linewidth is displayed in Fig. 5. The linewidth decreases with temperature below about 30°K, displays a weak minimum between 30 and 100°K, and then increases nonlinearly

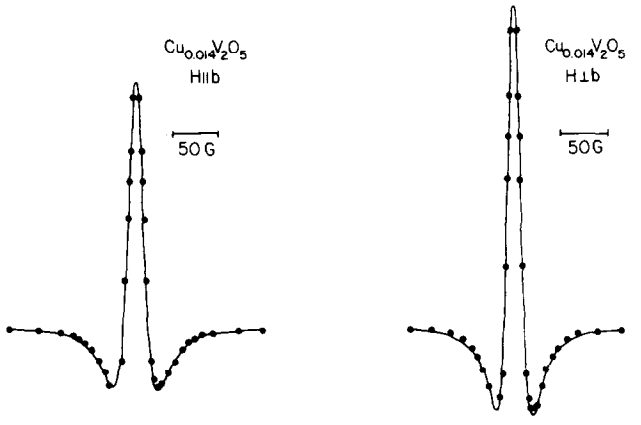

FIG. 1. Second-derivative EPR spectra for crystalline $Cu_{0.014}V_2O_5$ at 296°K for $H \| b$ and $H \perp b$. Solid circles are values computed from a Lorentzian lineshape function.

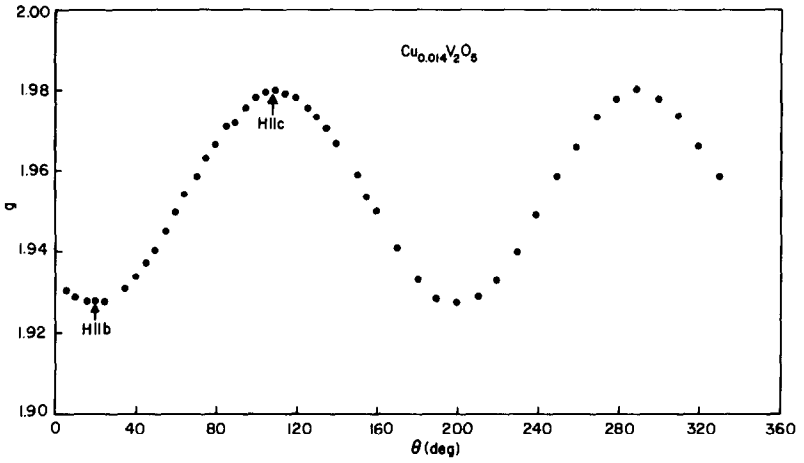

FIG. 2. Angular variation of the g-value in the b–c plane for crystalline $Cu_{0.014}V_2O_5$.

with temperature above about 100°K. The linewidth exhibits a similar orientation and temperature dependence in α-$Na_xV_2O_5$, α-$Li_xV_2O_5$ and V_2MoO_8. and the region in which the linewidth decreases with temperature was interpreted in terms of motional narrowing of the EPR signal by thermally activated hopping of the vanadium $3d'$ electron (*6*).

Within a rather large experimental error, the temperature dependence of the integrated intensities of the EPR lines followed the Curie law above 77°K.

2. Powdered $Cu_{0.010}V_2O_5$. The relative ease with which powder EPR spectra can be obtained led us to investigate the evaluation of EPR parameters from such spectra. A typical EPR spectrum of powdered

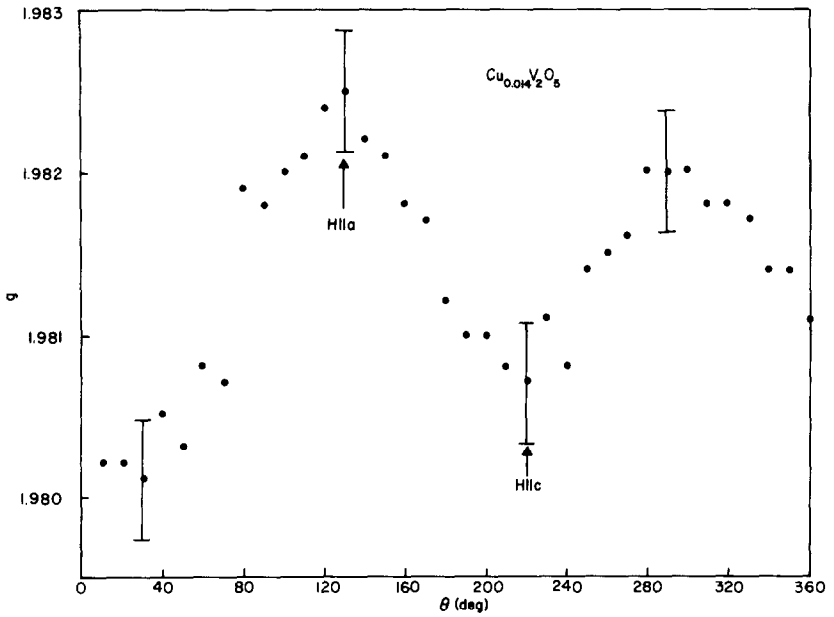

FIG. 3. Angular variation of the g-value in the a–c plane for crystalline $Cu_{0.014}V_2O_5$.

TABLE I

g-VALUES FOR $Cu_{0.01}V_2O_5$

Samples	g_x	g_y	g_z
Single crystal[a]	1.9825	1.9798	1.9279
Powder[b]	1.983	1.983	1.928

[a] Values obtained at 296°K. The error in each value is ±0.0004.

[b] Values obtained at 140°K. The error in each value is ±0.001.

$Cu_{0.01}V_2O_5$ is shown in Fig. 6. The appearance of the spectrum is characteristic of a powder having an axially symmetric g-tensor (*17, 18*). As shown in Fig. 6, the first-derivative EPR spectrum can be fitted reasonably well to the function

$$\frac{dI}{dx} = -\frac{A}{2ps^2}\left\{\frac{a\alpha}{s}\left[\frac{\pi}{2}+\tan^{-1}\left(\frac{p^2-s}{2bp}\right)\right] + \frac{b\beta}{2s}\ln\left(\frac{p^2+2ap+s}{p^2-2ap+s}\right) \pm \frac{2pd(2y\mp p^2)}{(p^4\mp 2p^2y+s^2)}\right\}, \quad (3)$$

where $x = \beta H/h\nu$, $c = 1/g$, $K = 2/\pi\Delta x$, $y = x - c_\perp$ $d = 1/\pi K$, $s = (y^2+d^2)^{1/2}$, $p = |c_\perp - c_\parallel|^{1/2}$, $a = (s/2 \pm y/2)^{1/2}$, $b = (s/2 \mp y/2)^{1/2}$, $\alpha = \pm 2y - s$, $\beta = \pm 2y + s$, where the upper sign applies to $C_\parallel > C_\perp$ and the lower sign to $C_\parallel < C_\perp$ (*17*). Equation (3) is valid if (a) each ion has axial symmetry, (b) the magnetic anisotropy is small, (c) the resonance lineshape for each crystallite is Lorentzian, (d) the crystallites are randomly oriented, (e) the spin Hamiltonian contains the Zeeman, dipolar, and exchange terms only, and (f) the linewidth for each crystallite is independent of orientation. Although assumptions (a)–(e) are valid, the linewidth does vary somewhat with orientation (see Fig. 4). Incorporation of the orientation dependence of the linewidth greatly complicates the computation of the lineshape function, and for powdered $Cu_{0.01}V_2O_5$ results in better agreement with experiment, but only a slight change in EPR parameters. Hence for the evaluation of EPR parameters in these solids it is not necessary to take into account the orientation dependence If the linewidth. Equation (3) was fitted to the experimental spectra by varying the g-values, $g_\parallel$ and $g_\perp$, and full width at half-maximum absorption, $\Delta H_{1/2}$, until the best least-squares fit was obtained. The resulting values of the EPR parameters at 140°K are

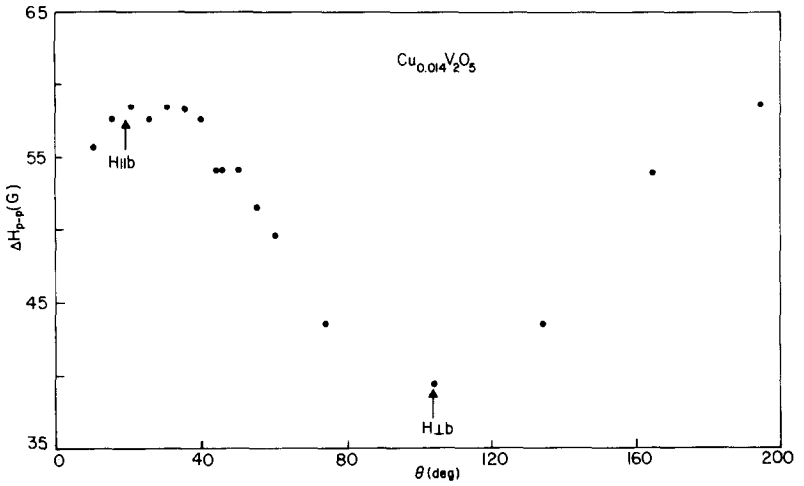

FIG. 4. Orientation dependence of the peak-to-peak linewidth in the b–c (or a) plane for crystalline $Cu_{0.014}V_2O_5$.

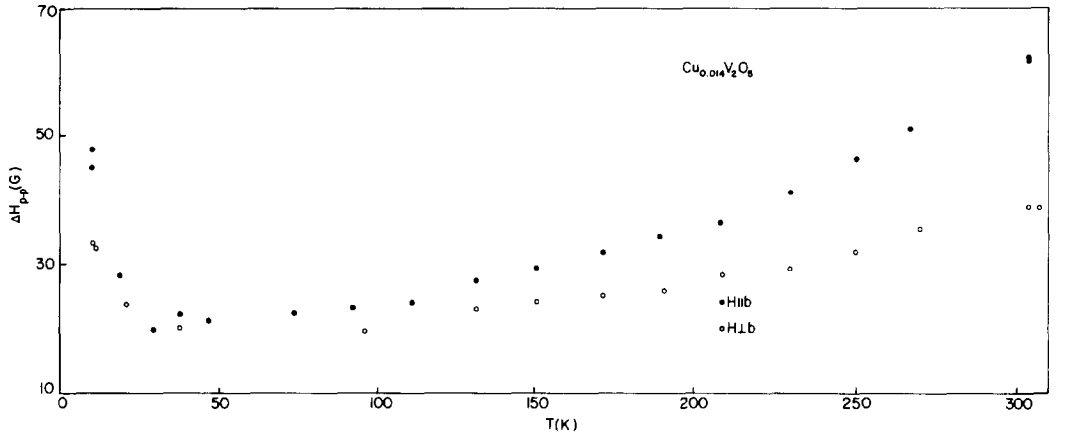

FIG. 5. Temperature dependence of the peak-to-peak linewidth of crystalline $Cu_{0.014}V_2O_5$ for $H \parallel b$ (solid circles) and $H \perp b$ (open circles).

summarized in Table I. The positions of the low-field and high-field peaks of the first-derivative curve can be used to determine $g_\parallel$ and $g_\perp$ to within about 1%.

In order to facilitate the determination of $\Delta H_{1/2}$ from the experimental spectra, theoretical spectra were calculated at various values of $\Delta H_{1/2}$ and the full width of the left lobe at half-power, $\Delta H'_{1/2}$, was measured. Assuming the temperature-independent values $g_\parallel = 1.928$ and $g_\perp = 1.983$ and $10\ \text{G} \leq \Delta H_{1/2} \leq 80\ \text{G}$, $\Delta H_{1/2}$ varied linearly with $\Delta H'_{1/2}$ according to the relation $\Delta H_{1/2} = 3\Delta H'_{1/2}/2 - 9/2$. The resulting temperature dependence of $\Delta H_{1/2}$ is shown in Fig. 7. The variation of linewidth with temperature is similar to that found in crystalline $Cu_{0.01}V_2O_5$.

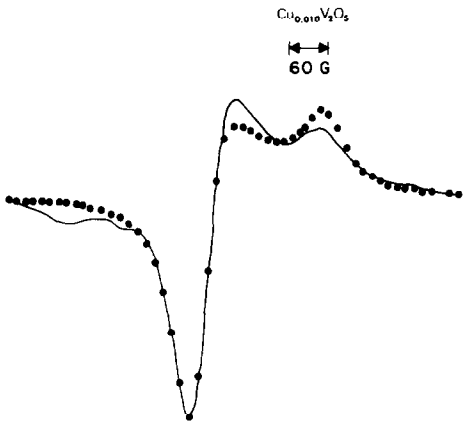

FIG. 6. First-derivative EPR spectrum of powdered $Cu_{0.01}V_2O_5$ at 140°K. Solid circles are values computed from Eq. (3) using the parameters in Table I.

B. Magnetic Susceptibility

1. Powdered $Cu_{0.010}V_2O_5$. The temperature dependences of the susceptibilities of the starting materials are shown in Figs. 8 and 9. Impurity paramagnetism occurs below about 30°K for both Cu and V_2O_5. For Cu, χ vs T^{-1} is linear below about 100°K, and the slope of this plot yields a Curie constant of 2.2×10^{-5} emu · deg/mole. Assuming that each impurity ion has one unpaired electron, then the impurity concetration is a negligible 60 ppm.

An independent run on a sample of Vanadium Corporation V_2O_5 showed a consistently larger susceptibility than that shown in Fig. 9, with the onset of paramagnetism occurring below about 80°K. For Johnson–Matthey V_2O_5, a plot of χ vs T^{-1} above about 60°K yielded a straight line with an infinite-temperature intercept of 104.5×10^{-6} emu/mole. This value of the temperature-independent paramagnetism of V_2O_5 is in reasonable agreement with previous

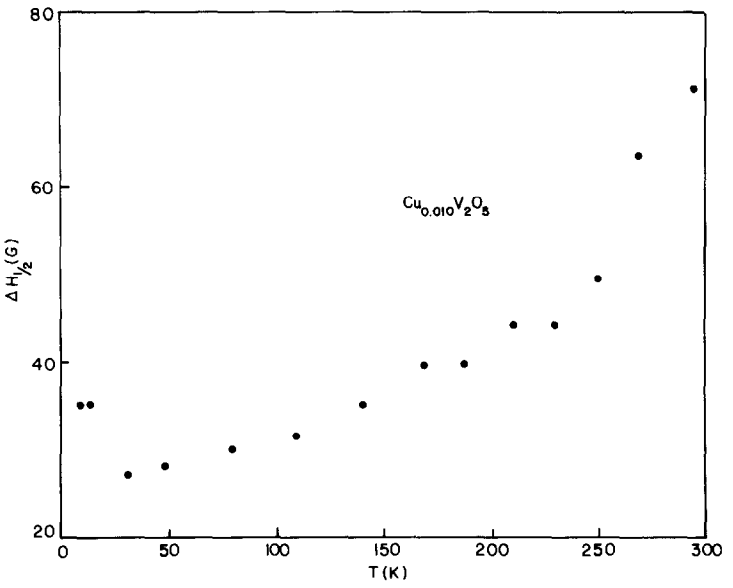

FIG. 7. Temperature dependence of the full-width at half-maximum absorption for powdered $Cu_{0.01}V_2O_5$.

determinations of 120×10^{-6} (*19*) and 112×10^{-6} emu/mole (*20*).

Since V_2O_5 makes a significant contribution to the susceptibility of $Cu_{0.01}V_2O_5$, sample susceptibilities were determined by subtracting the V_2O_5 and Cu^+ susceptibilities from the experimental susceptibilities:

$$\chi = \chi(\text{exp}) - \chi(V_2O_5) - \chi(Cu^+). \quad (4)$$

The temperature dependence of the resulting reciprocal molar susceptibility of powdered $Cu_{0.01}V_2O_5$ is shown in Fig. 10. Above about 100°K the susceptibility can be fitted to the Curie–Weiss law, $\chi = C/(T-\theta)$, where C and θ are the Curie and Weiss constants, respectively. C can be used to determine the magnetic moment $\mu = 2.828(C/x)^{1/2}\beta$, and θ is usually a measure of the interaction between these moments. The magnetic parameters of powdered $Cu_{0.01}V_2O_5$ are given in Table II.

2. Crystalline $Cu_{0.014}V_2O_5$. In analogy to the powder samples, the susceptibilities of

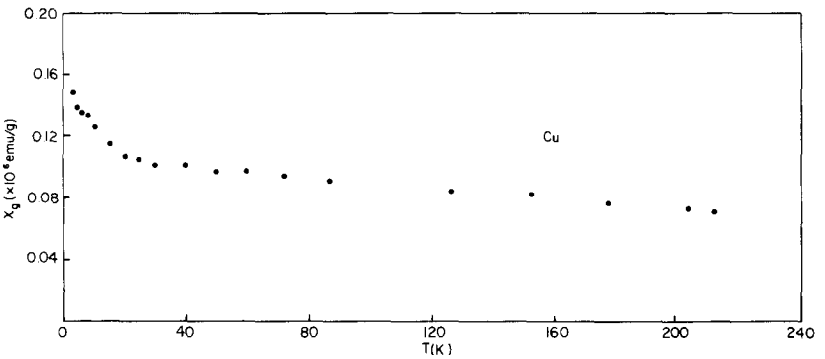

FIG. 8. Temperature dependence of the gram susceptibility of copper.

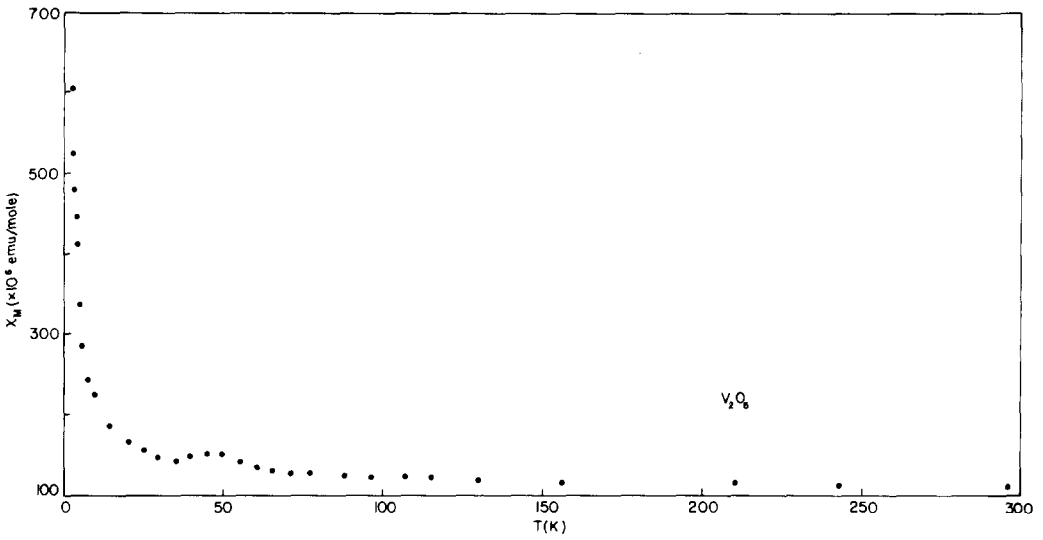

FIG. 9. Temperature dependence of the molar susceptibility of V_2O_5.

crystalline $Cu_{0.01}V_2O_5$ were calculated from the relation

$$\chi_r = \chi_r(\text{exp}) - \chi_r(V_2O_5) - \chi(Cu^+), \quad (5)$$

where $r = a$, b, c and χ_a, χ_b, and χ_c are the susceptibilities along three crystallographic axes. The reciprocal susceptibilities vs temperature for crystalline $Cu_{0.01}V_2O_5$ are shown in Figs. 11 and 12. Since $\chi_a = \chi_c$ within 5%, the susceptibility is nearly axially symmetric ($\chi_b = \chi_\parallel$, $\chi_a = \chi_c = \chi_\perp$) in agreement with the EPR results. The high-temperature magnetic data can be fitted to a Curie–Weiss law, and the magnetic parameters are given in Table II. Since $\chi_{\text{powder}} = \frac{1}{3}(\chi_\parallel + 2\chi_\perp)$ and $\mu_{\text{powder}} = [\frac{1}{3}(\mu_\parallel^2 + 2\mu_\perp^2)]^{1/2}$ within 10% over the entire temperature range, the powder and crystalline data are considered to be in excellent agreement considering the low doping level.

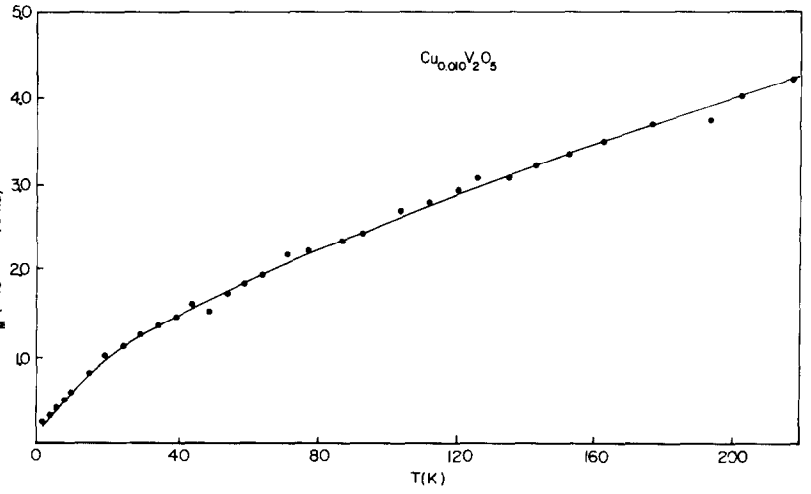

FIG. 10. Temperature dependence of the reciprocal molar susceptibility of powdered $Cu_{0.01}V_2O_5$.

TABLE II

MAGNETIC PARAMETERS FOR $Cu_{0.01}V_2O_5$

Sample	Orientation	C (emu · deg mole^{-1})	θ (°K)	μ (β (atom Cu^{-1}))
Powder		0.00727	−85	2.41
Single crystal	$H \parallel a$	0.0111	−54	2.52
	$H \parallel c$	0.0108	−48	2.48
	$H \parallel b$	0.00424	−67	1.56

Discussion

A. EPR

The good agreement between the crystalline and powder studies indicates that for these materials reasonably precise EPR parameters can be determined from less time-consuming and tedious experiments on powders.

The near-axial symmetry of the g-tensor follows from the structure of the α phase of $M_xV_2O_5$, which consists of tetragonally distorted VO_6 octahedra with the M cations occupying sites between the octahedra. The values of $g_\parallel$ and $g_\perp$ in $Cu_{0.01}V_2O_5$, and the fact that nearly the same values for these parameters were obtained by us for powdered α-$Li_{0.01}V_2O_5$ and α-$Na_{0.01}V_2O_5$ lead us to conclude, in agreement with other studies (*5,7*), that the paramagnetism is due to V^{4+}(3d′) and that copper is present as the diamagnetic cuprous ion $C^+(3d^{10})$. Since the local V^{4+} symmetry in α-$Cu_xV_2O_5$ is similar to that in $VO(H_2O)_5^{2+}$, the molecular-orbital calculations of Ballhausen and Gray (*21*) may be applicable. Their treatment indicates that the vanadium $3d_{xy}$ orbital, which is directed toward neighboring vanadium ions,

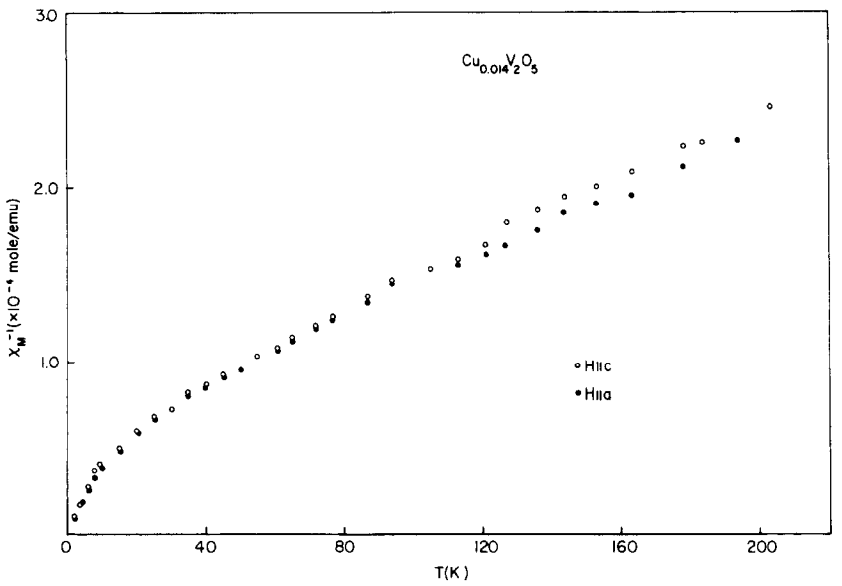

FIG. 11. Temperature dependence of the reciprocal molar susceptibility of crystalline $Cu_{0.014}V_2O_5$ for $H \parallel a$ (solid circles) and $H \parallel c$ (open circles).

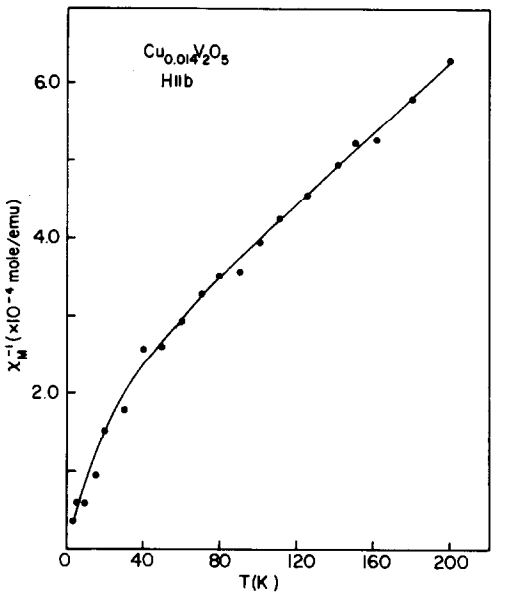

FIG. 12. Temperature dependence of the reciprocal molar susceptibility of crystalline $Cu_{0.014}V_2O_5$ for $H \parallel b$.

is the only nonbonding vanadium orbital and is also the lowest-lying partially filled orbital. The values of $g_\parallel$ and $g_\perp$ are consistent with a $3d_{xy}$ level as the ground state (*22*). A further discussion of the g-tensor will be given later in connection with the susceptibility studies.

Assuming that the vanadium–vanadium interactions are dipolar in nature, the full width at half-maximum absorption of the EPR lines in a powder can be estimated from the formula

$$\Delta H_d = 2f[\tfrac{3}{5}g^2\beta^2 S(S+1)\sum_{i\neq k} r_{ik}^{-6}]^{1/2}, \quad (6)$$

where f is the fraction of vanadium sites that are filled magnetically ($f<0.01$), $g = [\frac{1}{3}(g_\parallel^2 + 2g_\perp^2)]^{1/2}$, and r_{ik} is the distance between vanadium ions i and k (*23, 24*). Since $f = 0.005$, Eq. (6) should provide a lower limit for the dipolar width (*24*). Evaluation of Eq. (6) for $Cu_{0.01}V_2O_5$ results in a dipolar width ≥ 10 G, which is in rough agreement with experiment. Although the observed Lorentzian shape is expected at such small magnetic concentrations (*24*), the temperature dependence of the linewidth is unusual. A possible explanation of the linewidth behavior below 30°K is that the EPR lines are motionally narrowed by thermally activated hopping between vanadium sites, which would account for the Lorentzian shape and decrease in width with temperature. Furthermore, the lack of hyperfine structure found in several α-phase studies (*5–9*) would indicate that the hopping frequency ν of the localized, yet mobile, d electrons is larger than the hyperfine coupling constant in frequency units, i.e., $\nu \gtrsim 100$ MHz. For hopping from a single d orbital the linewidth should increase exponentially with T^{-1} according to the equation

$$\Delta H = \frac{\Delta H_d^2}{\Delta H_D}\exp(E_a/k_B T), \quad (7)$$

where ΔH_D is the Debye width and E_a is the activation energy for the hopping electron (*6*). A semilog plot of linewidth vs T^{-1} below 25°K for crystalline $Cu_{0.01}V_2O_5$ yields a straight line with $E_a = 0.010$ and 0.006 eV for $H \parallel b$ and $H \perp b$, respectively. These E_a's are well below the published values in α-$Cu_xV_2O_5$ of 0.08 eV along the c axis (*4*). Moreover, Eq. (7) cannot account for the minimum in the temperature dependence of the linewidth and the increase in linewidth with temperature above about 100°K.

The susceptibility studies discussed in the next section reveal that the V^{4+} in our samples has three thermally accessible excited states, with the magnetic moment of the lowest level being lower than that of the highest level and the moment of the intermediate level being quite small. Only the ground level contributes to the EPR signal, and we propose that thermally activated hopping is occurring from V^{4+} sites having thermally accessible excited states.[1] Then the low E_a's below 30°K suggest that motional

[1] Electrical conductivity measurements in α-$Cu_xV_2O_5$ do not reveal this behavior, but the small differences between the V^{4+} levels (~ 0.005 eV) would be very difficult to detect in such experiments.

narrowing is nearly complete in this range,[2] so that the variation in linewidth with temperature above 30°K reflects the thermal population of the V^{4+} levels. Above 30°K, the weakly magnetic intermediate level is increasingly occupied and the linewidth displays a minimum. As the temperature is increased further, the most magnetic upper level becomes occupied and the linewidth then increases with temperature.

The observed orientation dependence of the linewidth probably results from the anisotropy of the dipolar interaction (*23*).

B. Magnetic Susceptibility

Although the negative Weiss constants indicate an antiferromagnetic interaction between the V^{4+} moments above about 50°K, the susceptibility data provide no evidence for such ordering down to 2°K. Rather, the susceptibility increases with decreasing temperature more rapidly than predicted by the Curie–Weiss law. Hence we adopt the view that θ cannot be interpreted as an interaction constant and attempt to interpret the susceptibility data over the entire temperature range in terms of a temperature-dependent magnetic moment. This approach has been used to interpret the susceptibility on powdered sodium (*10*) and lithium (*11*) bronzes, but in both cases the magnetic analysis was incorrect, since V^{4+} was predicted to have a singlet ground state, which contradicts the observed rapid increase in susceptibility with decreasing temperature. Below we derive expressions for the temperature dependence of the magnetic moment, correct the magnetic analysis of the vanadium bronzes, and use the theory to interpret the magnetic and EPR data for powdered and crystalline $Cu_{0.01}V_2O_5$.

1. Theory. The EPR and susceptibility data have indicated that the ligand field at V^{4+} has axial symmetry, and, from the structure of V_2O_5, the symmetry of the oxygens about V^{4+} is approximately C_{4v}. Hence the problem reduces to one of calculating the susceptibility and moment of the $3d^{-1}$ electron of V^{4+} in an axially symmetric ligand field. We assume that exchange interactions between the moments are negligible and that the temperature dependence of the susceptibility for the V^{4+} moments arises from ordinary thermal disorder as well as from occupation of energy levels having different magnetic moments at each site. This problem has been treated numerically for powdered solids by Figgis (*25*), but here we present complete expressions for the moment in single crystals.

The appropriate Hamiltonian along one of the two principal directions $r = \parallel$ or $\perp$ in a crystal is

$$\hat{\mathcal{H}}_r = \hat{\mathcal{H}}_0 + (\hat{\mathcal{H}}_a)_r + \lambda_r(\hat{\mathbf{L}} \cdot \hat{\mathbf{S}})_r \qquad (8)$$

where λ_r is the spin–orbit coupling constant $\hat{\mathcal{H}}_0$ and $\hat{\mathcal{H}}_a$ are the Hamiltonians for the octahedral and axial fields, respectively. Briefly, the first term in Eq. (8) leads to the sixfold degenerate $^2T_{2g}$ term of the octahedral field being lowest,[3] and the combined purturbation of the remaining terms splits the $^2T_{2g}$ levels into three doubly degenerate levels,

$$\begin{aligned}
[\Gamma_7(E)]_r &= 1/2(-\Delta/3 + \lambda_r/2 + \xi_r), \\
[\Gamma_7(B)]_r &= 1/2(-\Delta/3 + \lambda_r/2 - \xi_r), \\
[\Gamma_6(E)]_r &= \Delta/3 - \lambda_r/2, \qquad (9)
\end{aligned}$$

where the axial distortion Δ is the separation between the orbital levels of $^2T_{2g}$ in the absence of spin–orbit coupling, and $\xi_r = (\Delta^2 + \Delta\lambda_r + 2.25\lambda_r^2)^{1/2}$. The axial field splits the $^2T_{2g}$ term into a twofold degenerate B level and a fourfold degenerate E level, and the spin–orbit coupling splits the E level into two twofold degenerate levels. The magnetic moment operator is taken to be

[2] Such motional narrowing can occur at very low temperatures in partially reduced vanadium oxides. In V_2MoO_8 line narrowing occurs below 4°K (*6*).

[3] The $^2T_2$ term is lowest for a d^1 ion in an octahedral field, for a d^9 ion in a tetradedral field, and for a d^5 ion in a strong octahedral field. The expressions given in this section are applicable in these three situations.

$(\hat{\boldsymbol{\mu}}_r = (k_r\hat{\boldsymbol{L}}_r + 2\hat{\boldsymbol{S}}_r)\beta$, where the orbital reduction parameter k gives the fraction of the time that the d electron is localized on the metal cation. Then the Van Vleck formula [26],

$$\chi_r = N\sum_i \{[W_i^I)_r]^2/k_BT - 2(W_i^{II})_r\} \frac{\exp[-(W^\circ{}_i)_r/k_BT]}{\sum_i \exp[-W^\circ{}_i)_r/k_BT]} \quad (10)$$

where $(W^\circ{}_i)_r$ is the energy in the absence of a magnetic field (given by Eqs. (9), the first-order Zeeman coefficient $(W_i^I)_r = \langle i|(\hat{\boldsymbol{\mu}})|_r|i\rangle$, and the second-order Zeeman coefficient

$$(W_i^{II})_r = \sum_{j\neq i} |\langle i|(\hat{\boldsymbol{\mu}})_r|j\rangle|^2/[(W^\circ{}_i)_r - (W^\circ{}_j)_r],$$

can be used to calculate the susceptibility and effective magnetic moment $\mu_r = (3k_BT\chi_r/N\beta^2)^{1/2}$. The resulting magnetic moments of the individual levels are given by

$$(\mu_\parallel{}^2)_{\Gamma_7(E)} = 3\left(\frac{k_\parallel + 1 - \alpha_\parallel^2}{1+\alpha_\parallel^2}\right)^2 - \frac{12k_B(k_\parallel + 1 - \alpha_\parallel\gamma_\parallel)^2}{(1+\alpha_\parallel^2)(1+\gamma_\parallel^2)\xi_\parallel} T,$$

$$(\mu_\perp{}^2)_{\Gamma_7(E)} = 3\left(\frac{2^{1/2}\alpha_\perp k_\perp - \alpha_\perp}{1+\alpha_\perp^2}\right)^2 - \frac{24k_B}{(1+\alpha_\perp^2)\lambda_\perp} \left[\frac{(\alpha_\perp k_\perp/2^{1/2} + \gamma_\perp k_\perp/2^{1/2} - \alpha_\perp\gamma_\perp)^2}{2(1+\gamma_\perp^2)\delta_\perp} - \frac{(1-\alpha_\perp k_\perp/2^{1/2})^2}{(v_\perp - 3/2 - \delta_\perp)}\right] T,$$

$$(\mu_\parallel{}^2)_{\Gamma_7(B)} = 3\left(\frac{k_\parallel + 1 - \gamma_\parallel^2}{1+\gamma_\parallel^2}\right)^2 + \frac{12k_B(k_\parallel + 1 - \alpha_\parallel\gamma_\parallel)^2}{(1+\alpha_\parallel^2)(1+\gamma_\parallel^2)\xi_\parallel} T,$$

$$(\mu_\perp)_{\Gamma_7(B)} = 3\left(\frac{2^{1/2}\gamma_\perp k_\perp - \gamma_\perp^2}{(1+\gamma_\perp^2)}\right)^2 + \frac{24k_B}{(1+\gamma_\perp^2)\lambda_\perp} \left[\frac{(\alpha_\perp k_\perp/2^{1/2} + \gamma_\perp k_\perp/2^{1/2} - \alpha_\perp\gamma_\perp)^2}{2(1+\alpha_\perp^2)\delta_\perp} + \frac{(1-\gamma_\perp k_\perp/2^{1/2})^2}{(v_\perp - 3/2 + \delta_\perp)}\right] T,$$

$$(\mu_\parallel{}^2)_{\Gamma_6(E)} = 3(1-k_\parallel)^2,$$

$$(\mu_\perp{}^2)_{\Gamma_6(E)} = -\frac{24k_B}{(v_\perp - 3/2 + \delta_\perp)\lambda_\perp} \left[\frac{(1-\alpha_\perp k_\perp/2^{1/2})^2}{(1+\alpha_\perp^2)} + \frac{(1-\gamma_\perp k_\perp/2^{1/2})^2}{(1+\gamma_\perp^2)}\right] T, \quad (11)$$

where $\alpha_r = (\frac{1}{2} + v_r - \delta_r)/2^{1/2}$, $\gamma_r = (\frac{1}{2} + v_r + \delta_r)/2^{1/2}$, $\delta_r = \xi_r/\lambda_r$, and $v_r = \Delta/\lambda_r$. In each of the above equations the temperature-indpendent term arises from the first-order Zeeman effect, whereas the term varying linearly with temperature is due to the second-order Zeeman effect. It should be noted that the moment of the $\Gamma_6(E)$ level is small and vanishes to first order if $k_\parallel = 1$. Applying Eq. (10), the calculated effective moments are

$$\mu_\parallel{}^2 = \frac{3\left\{(k_\parallel - 1)^2 \exp[-(v_\parallel/3 - 1/2)/x_\parallel] + \left[\left(\frac{k_\parallel + 1 - \alpha_\parallel^2}{1+\alpha_\parallel^2}\right)^2 - \frac{2x_\parallel(k_\parallel + 1 - \alpha_\parallel\gamma_\parallel)^2}{(1+\alpha_\parallel^2)(1+\gamma_\parallel^2)\delta_\parallel}\right] \exp[-(1/2 - v_\parallel/3 + \delta_\parallel)/2x_\parallel] + \left[\left(\frac{k_\parallel + 1 - \gamma_\parallel^2}{1+\gamma_\parallel^2}\right)^2 + \frac{2x_\parallel(k_\parallel(k_\parallel + 1 - \alpha_\parallel\gamma_\parallel)^2}{(1+\alpha_\parallel^2)(1+\gamma_\parallel^2)\delta_\parallel}\right] \exp[-(1/2 - v_\parallel/3 - \delta_\parallel)/2x_\parallel]\right\}}{\exp[-(v_\parallel/3 - 1/2)/x_\parallel] + \exp[-(1/2 - v_\parallel/3 + \delta_\parallel)/2x_\parallel] + \exp[(1/2 - v_\parallel/3 - \delta_\parallel)/2x_\parallel]},$$

$$3\left[-4x_\perp\left[\frac{(1-\alpha_\perp k_\perp/2^{1/2})^2}{(1+\alpha_\perp)^2(v_\perp-3/2-\delta_\perp)}+\frac{(1-\gamma_\perp k_\perp/2^{1/2})^2}{(1+\gamma_\perp^2)(v_\perp-3/2+\delta_\perp)}\right]\right.$$

$$\exp[-(\nu_\perp/3-1/2)/x_\perp]+\left\{\left(\frac{2^{1/2}\alpha_\perp\times k_\perp-\alpha_\perp^2}{1+\alpha_\perp^2}\right)^2\right.$$

$$\left.-\frac{4x_\perp}{(1+\alpha_\perp^2)}\left[\frac{(\alpha_\perp k_\perp/2^{1/2}+\gamma_\perp k_\perp/2^{1/2}-\alpha_\perp\gamma_\perp)^2}{2(1+\gamma_\perp^2)\delta_\perp}-\frac{(1-\alpha_\perp k_\perp/2^{1/2})^2}{(v_\perp-3/2-\delta_\perp)}\right]\right\}$$

$$\exp[-(1/2-v_\perp/3+\delta_\perp)/2x_\perp]+\left\{\left(\frac{2_\perp^{1/2}k_\perp-\gamma_\perp^2}{1+\gamma_\perp^2}\right)^2\frac{4x_\perp}{(1+\gamma_\perp^2)}\right.$$

$$\left.\left[\frac{(\alpha_\perp k_\perp/2^{1/2}+\gamma_\perp k_\perp/2^{1/2}-\alpha_\perp\gamma_\perp)^2}{2(1+\alpha_\perp^2)\delta_\perp}+\frac{(1-\gamma_\perp k_\perp/2^{1/2}}{(v_\perp-3/2+\delta_\perp)}\right]\right\}\exp[-(1/2-v_\perp/3-\delta_\perp)/2x_\perp]$$

$$\mu_\perp{}^2=\frac{}{\exp[-(v_\perp/3-1/2)/x_\perp]+\exp[-(1/2-v_\perp/3+\delta_\perp)/2x_\perp]+\exp[-1/2-v_\perp/3-\delta_\perp)/2x_\perp]},$$

(12)

where $x_r = kT/\lambda_r$. The powder susceptibility χ and moment μ_{eff} can be calculated from the above equations by using the formulas $\chi = (\chi_\parallel + 2\chi_\perp)/3$ and $\mu_{\text{eff}} = [\frac{1}{3}(\mu_\parallel^2 + 2\mu_\parallel^2)]^{1/2}$. The above expressions yield the numerical results of Figgis (*25*) when k and λ are isotropic. Only k, λ, and Δ can be determined from the susceptibility of powders. Crystalline susceptibility data are required for evaluation of the anisotropy in k and λ. In either case values of the ligand-field parameters can be extracted from a least-squares fit of the above theoretical expressions to the experimental data.

2. Discussion. The best-fit values of the ligand-field parameters for powdered and crystalline $Cu_{0.01}V_2O_5$ are summarized in Table III, and Figs. 13–15 show the agreement between the calculated and experimental moments. The resulting energy-level diagram for powdered $Cu_{0.01}V_2O_5$ is displayed in Fig. 16. The crystalline material had the same sequence of levels as shown in Fig. 16.

TABLE III

LIGAND-FIELD PARAMETERS FOR $Cu_{0.01}V_2O_5$

Sample	Orientation	k[a]	λ (eV)	Δ (eV)
Powder		1.0	0.008	0.014
Single crystal	$H \perp b$	1.0	0.004	0.008
	$H \parallel b$	0.5	0.024	0.005

[a] The errors in k, λ, and Δ are 0.1, 0.002 eV, and 0.003 eV, respectively.

A limiting case of the theory is to determine the moment at low temperatures, where only the ground state is appreciably occupied. Using the parameters in Table III for powdered $Cu_{0.01}V_2O_5$, below 20°K the moment should lie between 1.1 and 1.3 β. Figure 17 shows a least-squares fit of the reciprocal susceptibility vs temperature for powdered $Cu_{0.01}V_2O_5$ to the Curie–Weiss law below 20°K. The resulting moment is $1.39 \pm 0.09\,\beta$, which is in reasonable agreement with the theoretical moment. Using the parameters in Table III, similar good agreement between the theoretical and experimental moments below 20°K is obtained for crystalline $Cu_{0.01}V_2O_5$.

For powdered $Cu_{0.01}V_2O_5$, the value $k = 1.0$ indicates that the paramagnetic d electron is localized on a single vanadium ion, which implies that the time spent by each d electron on a vanadium site is long compared to the duration of a hop. The marked devia-

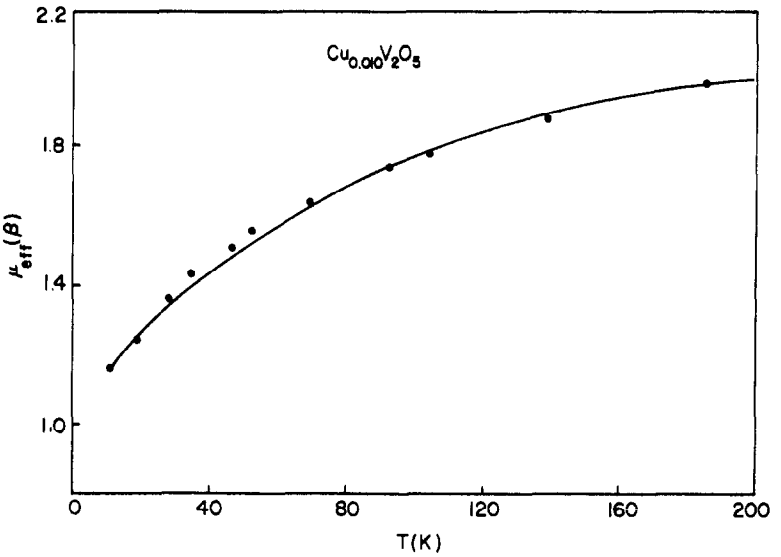

FIG. 13. Comparison of the experimental (solid circles) and theoretical (solid curve) moments as a function of temperature for powdered $Cu_{0.01}V_2O_5$. The solid curve was calculated using $k = 1.0$, $\lambda = 0.008$ eV, and $\Delta = 0.014$ eV.

tion of λ from the free-ion value (0.0312 eV) suggests that the effective nuclear charge of vanadium has been reduced as a result of covalent bonding with the surrounding oxygens. The small, positive value of Δ indicates a slightly compressed C_{4v} symmetry. This suggests that the axial compression arising from the shortest V–O bond (1.54 Å) is nearly compensated for by the axial expansion resulting from the opposite, longest V–O bond (2.83 Å). The values of the ligand-field parameters are comparable to

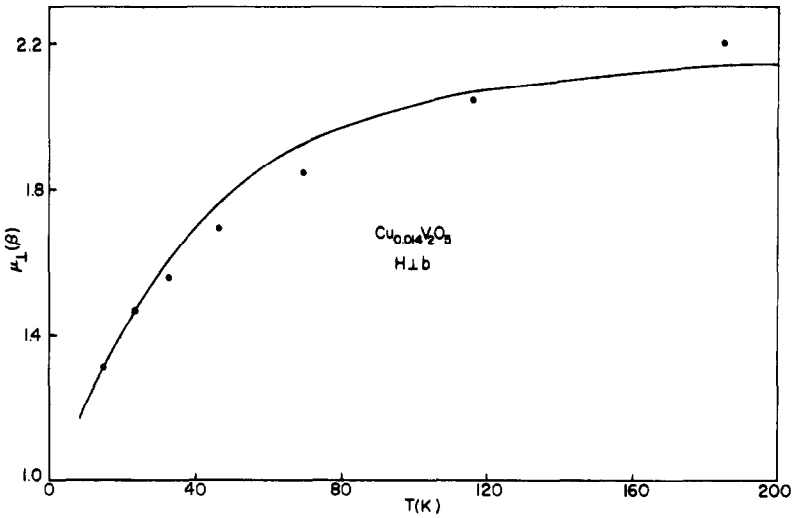

FIG. 14. Comparison of the experimental (solid circles) and theoretical (solid curve) moments as a function of temperature for crystalline $Cu_{0.014}V_2O_5$ for $H \perp b$. The solid curve was calculated using $k = 1.0$, $\lambda = 0.004$ eV, and $\Delta = 0.008$ eV.

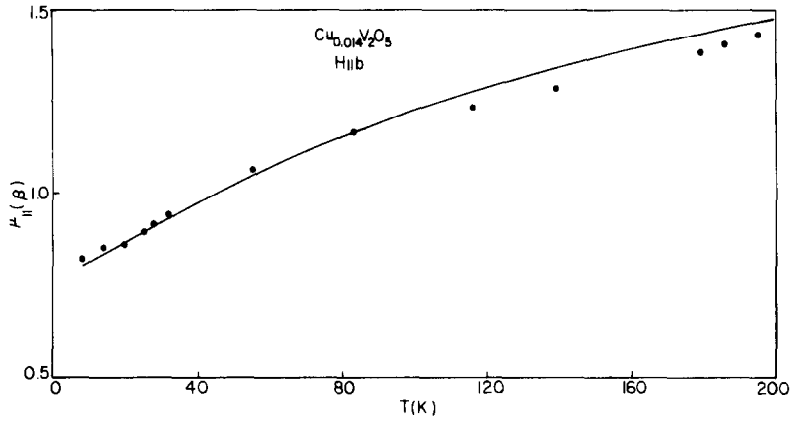

FIG. 15. Comparison of the experimental (solid circles) theoretical (solid curve) moments as a function of temperature for crystalline $Cu_{0.014}V_2O_5$ for $H \parallel b$. The solid curve was calculated using $k = 0.5$, $\lambda = 0.024$ eV, and $\Delta = 0.003$ eV.

those found in powdered $Li_{0.25}V_2O_5$ (*11*). However, in contrast to $Li_{0.25}V_2O_5$, we find that the magnetic $\Gamma_7(B)$ level lies lowest, followed by the weakly magnetic $\Gamma_6(E)$ and magnetic $\Gamma_7(E)$ levels, with $(\mu_{eff})_{\Gamma_7}(E) > (\mu_{eff})_{\Gamma_7}(B)$. These results are consistent with the low-temperature susceptibility data, since the susceptibility should increase with decreasing temperature upon depopulation of the weakly magnetic $\Gamma_6(E)$ level and occupation of the magnetic $\Gamma_7(B)$ level. Inspection of the previous vanadium-bronze studies reveals that the $\Gamma_6(E)$ and $\Gamma_7(B)$ levels should be interchanged, which results in the same level sequence as shown in Fig. 16 and yields consistency with the experimental susceptibility data.

For crystalline $Cu_{0.01}V_2O_5$, the values of $k_\perp$, $\lambda_\perp$, and Δ are in reasonable agreement with the powder results. However, the small value of $k_\parallel = 0.5$ indicates an appreciable delocalization of the paramagnetic d electron onto the oxygen ligands along the b axis, which probably results from overlap of the V($3d$) and O($p\pi$) orbitals. The proximity of $\lambda_\parallel$ to the free-ion value may result from ineffective screening of the vanadium nuclear charge by the electrons in the long V–O bond (2.83 Å) along the b axis.

It is of interest to compare the susceptibility and EPR results. The Curie behavior of the EPR signal and temperature independence of the g-tensor indicate that only the $\Gamma_7(B)$ ground level contributes to the EPR signal. Since the $\Gamma_7(B)$ wave functions are equivalent to those of $3d_{xy}$, the $\Gamma_7(B)$ ground level is supported by the g-tensor results. Although the finding of

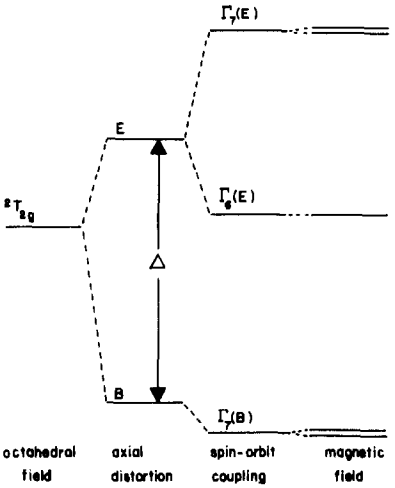

FIG. 16. Energy-level diagram for powdered $Cu_{0.01}V_2O_5$ showing the effects of axial distortion, spin–orbit coupling, and magnetic field on the $^2T_{2g}$ ground term of the octahedral field.

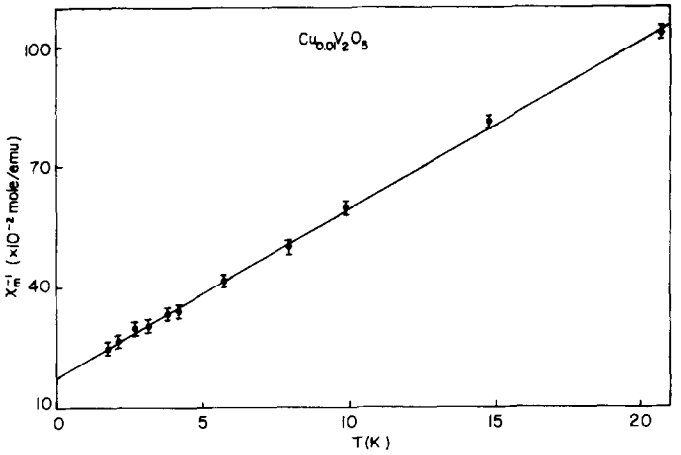

FIG. 17. Reciprocal molar susceptibility vs temperature for powdered $Cu_{0.01}V_2O_5$ below 20°K.

significant V–O π bonding along the *b*-direction is in apparent contradiction to the nonbonding nature of the $3d_{xy}$ orbital, we emphasize that the VO_6 octahedra are extremely distorted, and our model of an axial distortion of an octahedral complex along the *b* direction is only a rough approximation, in which case such π bonding is not precluded. Abragam and Bleaney (*27*) have given expressions for $g_\parallel$ and $g_\perp$ for both isotropic and anisotropic k and λ. Using the parameters in Table III, we find for the ground level in the isotropic case that $g_\parallel = 1.54 \pm 0.03$ and $g_\perp = 1.09 \pm 0.03$ and in the anisotropic case that $g_\parallel = 1.90 \pm 0.07$ and $g_\perp = 1.57 \pm 0.21$. The anisotropic parameters are clearly in better agreement with experiment. The energy-level scheme is similar to that given in Fig. 16, with magnetic ground and highest levels and a weakly magnetic intermediate level.

Conclusion

In this study we have developed a self-consistent model of the magnetic behavior of α-$Cu_xV_2O_5$ near the compositional limit. The EPR results show that V^{4+} is in an axially symmetric environment and that the EPR line is motionally narrowed by thermally activated hopping of the paramagnetic electron between vanadium sites. The susceptibility data are interpreted in terms of a ligand-field model, which results in magnetic ground and highest levels and a weakly magnetic intermediate level. This model not only accounts for the susceptibility data, but also explains the main features of the *g*-tensor and the temperature dependence of the linewidth.

The equivalent V^{4+} centers studied here are apparently different than those studied by others at lower compositions, where different vanadium centers and delocalization of the paramagnetic electron over more than one vanadium center are observed. A detailed EPR study as a function of composition is required to resolve the evolution of paramagnetic centers in these solids with increasing x.

Finally, we comment upon the catalytic implications of our results. The longest and shortest V–O bonds occur in the *b* direction. Because the longest V–O bond is weaker then the other V–O bonds, V_2O_5 as well as partially reduced V_2O_5 cleaves preferentially perpendicular to the *b* axis, which exposes the vanadyl oxygen on the surface. This V–O bond has the character of a double bond and hence should be more reactive than the other

V–O bonds. It is this more reactive vanadyl oxygen that may play an important role in oxidation catalysis by V_2O_5. An important observation is that the surface reactivity of V_2O_5 is increased considerably upon partial reduction (*28*). This enhanced reactivity may be due in part to the increased electron density in the shortest V–O bond due to the π bonding of the paramagnetic electron with the vanadyl oxygen.

Given a negligible exchange interaction between the vanadium moments, the magnetic analysis used in this paper should be applicable to V^{4+} in other partially reduced vanadium pentoxides, and in particular the vanadium bronzes. In the following two papers we successfully employ this approach to study β'-$Cu_xV_2O_5$, which has been reported to exhibit a continuous semiconductor → metal transition with increasing x, and $(Mo_xV_{1-x})_2O_5$, which is a useful oxidation catalyst.

References

1. A. HARDY, J. GALY, A. CASALOT, AND M. POUCHARD, *Bull. Soc. Chim. Fr.*, 1056 (1965).
2. A. BYSTRÖM, K. A. WILHELMI, AND O. BROTZEN, *Acta Chem. Scand.* **4**, 1119 (1950).
3. J. GALY, J. DARRIET, A. CASALOT, AND J. B. GOODENOUGH, *J. Solid State Chem.* **1**, 339 (1970).
4. J. H. PERLSTEIN, *J. Solid State Chem.*. **3**, 217 (1971).
5. J. L. RAGLE *J. Chem. Phys.* **38**, 2020 (1963).
6. G. SPERLICH, *Z. Phys.* **250**, 335 (1972).
7. G. SPERLICH AND W. D. LAZÉ, *Phys. Status Solidi B* **65**, 625 (1974).
8. G. GILLIS AND E. BOESMAN, *Phys. Status Solidi* **14**, 337 (1966).
9. E. BOESMAN AND G. GILLIS, *Phys. Status Solidi* **14**, 349 (1966).
10. J. H. PERLSTEIN AND M. J. SIENKO, *J. Chem. Phys.* **48**, 174 (1968).
11. H. KESSLER AND M. J. SIENKO, *J. Solid State Chem.* **1**, 152 (1970).
12. J. B. GOODENOUGH, *J. Solid State Chem.* **1**, 349 (1970).
13. W. S. GLAUNSINGER, *J. Phys. E* **8**, 996 (1975).
14. D. A. GORDON, R. F. MARZKE, AND W. S. GLAUNSINGER, *J. Phys. (Paris)* **7**, C2–87 (1977).
15. W. S. GLAUNSINGER AND M. J. SIENKO, *J. Chem. Phys.* **62**, 1883 (1975).
16. N. J. VANA AND E. UNFRIED, *J. Magn. Reson.* **6**, 655 (1972).
17. J. W. SEARL, R. C. SMITH, AND S. J. WYARD, *Proc. Phys. Soc. London Sect. A* **74**, 491 (1959).
18. J. A. IBERS AND J. D. SWALEN, *Phys. Rev.* **127**, 1914 (1962).
19. M. POUCHARD, A CASALOT, G. VILLENEUVE, AND P. HAGENMULLER, *Mat. Res. Bull.* **2**, 877 (1967).
20. M. J. SIENKO AND J. B. SOHN, *J. Chem. Phys.* **44**, 1369 (1966).
21. C. J. BALLHAUSEN AND H. B. GRAY, *Inorg. Chem.* **1**, 111 (1962).
22. D. KIVELSON AND S. LEE, *J. Chem. Phys.* **41**, 1896 (1964).
23. J. H. VAN VLECK, *Phys. Rev.* **74**, 1168 (1948).
24. C. KITTEL AND E. ABRAHAMS, *Phys. Rev.* **90**, 238 (1953).
25. B. N. FIGGIS, *Trans, Faraday Soc.* **57**, 198 (1961)
26. J. H. VAN VLECK, "Theory of Electric and Magentic Susceptibilities," p. 182, Oxford Univ. Press, London/New York (1932).
27. A. ABRAGAM AND B. BLEANEY, "Electron Paramagnetic Resonance of Transition Ions," Chap. 7, Oxford Univ. Press, London/New York (1970).
28. M. N. COLPAERT, P. CLAUWS, L. FIERMANS, AND J. VENNIK, *Surface Sci.* **36**, 513 (1973).